Thermal, Conductivity, NMR, and Raman Spectroscopic Measurements and Phase Diagram of the $Cs_2S_2O_7$−$CsHSO_4$ System

Søren B. Rasmussen,[†,‡] Hind Hamma,[§] Olga B. Lapina,[||] Dzhalil F. Khabibulin,[||] K. Michael Eriksen,[†,‡] Rolf W. Berg,[†] Gerard Hatem,[§,⊥] and Rasmus Fehrmann*[,†,‡]

Department of Chemistry, Technical University of Denmark, DK-2800 Lyngby, Denmark, ICAT (Interdisciplinary Research Centre for Catalysis), Technical University of Denmark, DK-2800 Lyngby, Denmark, UMR-CNRS, TECSEN, Avenue Escadrille Normandie Niemen, Faculté des Sciences, St Jérôme 13397, Marseille Cedex 20, France, and Boreskov Institute of Catalysis, Prospekt Lavrentiva 5, Novosibirsk 630090, Russia

Received: April 29, 2003; In Final Form: September 26, 2003

The conductivity of the binary system $Cs_2S_2O_7$−$CsHSO_4$ has been measured at 20 different molten compositions in the full composition range and in the temperature range 430−750 K. From the obtained liquidus−solidus phase transition temperatures, the phase diagram has been constructed. It is of the simple eutectic type with the composition $X(CsHSO_4) = 0.86$ and temperature of fusion of 470 K for the eutectic. The previously unpublished temperature of fusion of $CsHSO_4$ was found to be 491.7 K. The experimental phase diagram is in good accordance with a calculated diagram based on measured thermodynamic properties of the pure compounds and the heat of liquid−liquid mixing measured for $X(CsHSO_4) = 0.5$ and 1.0. ^{133}Cs and ^{17}O NMR spectra and Raman spectra of the liquid $Cs_2S_2O_7$−$CsHSO_4$ system indicate the presence of a temperature sensitive equilibrium $2HSO_4^- \rightleftharpoons S_2O_7^{2-} + H_2O$ where the water molecules are strongly associated in the melt. Fast exchange reactions take place between the species present, leading to the observed ^{17}O NMR single line with an averaged chemical shift. Super-ionic and thermodynamic stable phases and the temperatures of phase transitions have been identified from the NMR measurements on $CsHSO_4$, $Cs_2S_2O_7$, and $Cs_2S_2O_7$−$CsHSO_4$ mixtures. For 11 selected compositions covering the entire composition range of the $Cs_2S_2O_7$−$CsHSO_4$ binary system, the conductivity of the molten state has been expressed by equations of the form $\kappa(X) = A(X) + B(X)(T - T_m) + C(X)(T - T_m)^2$ where T_m is the intermediate temperature of the measured temperature range and X is the initial mol fraction of $CsHSO_4$.

Introduction

The SO_2 oxidation process is mainly used for sulfuric acid production and the working catalyst is usually described chemically by the model melt system $M_2S_2O_7/V_2O_5$ (M = alkali metal) in steady-state equilibrium with a $SO_2/O_2/SO_3/N_2$ gas mixture.

During the past decades, cesium has been introduced as a promoter for the commercial supported liquid phase (SLP) catalyst for SO_2 oxidation. The use of alkali cations such as Na^+, K^+, and Cs^+ enhances the catalytic activity of vanadium by forming molten pyrosulfates, $S_2O_7^{2-}$, where vanadium complexes are formed at process conditions. This is due to the presence of SO_3 in the gas phase reacting with the vanadium and alkali oxides formally present on the surface of the supported catalyst, forming the pyrosulfate melt and the dissolved oxo sulfato vanadates.

With the increasing restrictions on allowed emission of SO_2, the oxidation process is now also used for removal of SO_2 from power plant flue gases. Given the change in gas components, the catalyst solvent is best described by the model melt system $M_2S_2O_7/MHSO_4$, because the presence of water in the system leads to an equilibrium (eq 1) between H_2O, $S_2O_7^{2-}$, and HSO_4^-

$$S_2O_7^{2-} + H_2O \leftrightarrows 2HSO_4^- \quad (1)$$

Previously, we have reported phase diagrams and properties for the binary systems $M_2S_2O_7$−$MHSO_4$ (M = Na[1] and K[2]) and published several investigations regarding spectroscopic and thermodynamic properties of the pure components (see ref 3 and references therein). $Cs_2S_2O_7$ has been thoroughly investigated by numerous methods especially in relation to its complex formation and mixing properties with vanadium pentoxide.[4−11]

Reports on $CsHSO_4$ only deal with the solid state in the temperature region of 18−450 K. The compound has a solid−solid transition at 417 K. The high-temperature phase is a quasi liquid state of cyclic dimers instead of the linear chains present in the low-temperature phase. The quasi liquid phase exhibits the properties of a super-ion conductor that has possible electrochemical appliances. As for $CsHSO_4$ in the liquid state, relevant to the catalytic deSOx process, very little has been reported in the literature.

In this work, we present measurements of thermodynamic and structural properties of the binary system obtained by use of several methods suitable for characterization of molten salt systems, i.e., electrical conductivity, Raman spectroscopy, NMR spectroscopy, and thermal methods.

* To whom correspondence should be addressed. E-mail: rf@kemi.dtu.dk.
† Department of Chemistry, Technical University of Denmark.
‡ ICAT (Interdisciplinary Research Centre for Catalysis), Technical University of Denmark.
§ UMR-CNRS, TECSEN.
|| Boreskov Institute of Catalysis.
⊥ Deceased.

10.1021/jp030535p CCC: $25.00
Published on Web 11/21/2003

Experimental Section

Chemicals. Pure $Cs_2S_2O_7$ was made by thermal decomposition of $Cs_2S_2O_8$, synthesized as earlier described.[4] Pure $CsHSO_4$ was synthesized by carefully adding weighed amounts of water into an ampule with $Cs_2S_2O_7$ which then was cooled (to lower the water vapor pressure) and sealed. The sample was thereafter heated and cooled in several cycles until the reaction was completed. All other handling of chemicals was performed in a glovebox with a H_2O content less than around 10 ppm. Samples were sealed immediately after filling.

Conductivity Measurements. The construction of and experimental details concerning the borosilicate cell with two gold electrodes fused vacuum tight through the glass walls have earlier been described.[2] The cell was placed in a furnace, which was regulated within ±0.1 K, at the highest measuring temperature. The conductivity was then measured at several temperatures during stepwise decrease of the temperature until crystallization occurred usually after subcooling of the melt. Thereafter, a series of measurements were obtained by stepwise increase of the temperature and the solidus point could be identified by observing a dramatic increase in conductivity occurring when the system transforms from a solid phase into a two-phase system. The liquidus point was thereafter observed as the temperature where the conductivity coincided with the conductivity obtained during the decrease of the temperature.

Thermal Measurements. The partial enthalpies of mixing of $Cs_2S_2O_7$ in $CsHSO_4$ in the binary system was measured by using a Calvet micro calorimeter. Measurements were carried out by breaking fragile ampules with $Cs_2S_2O_7$ in the $Cs_2S_2O_7$−$CsHSO_4$-melt containing crucibles (after the ampules had been thermally equilibrated). The calibration of the calorimeter was performed after each experiment by dropping pure gold (5 N) samples in the same experimental cell.

The melting point of the eutectic was controlled by DTA measurements. The apparatus was a DSC 111 from Setaram. The heating rate was 2 K s^{-1}.

NMR Spectroscopy. NMR spectra were measured on a Bruker MSL-400 spectrometer with a magnetic field of 9.4 T.

The measurements at high temperatures, i.e., up to 750 K, were performed with a homemade high-temperature probe. The probe consisted of a 60 mm long and 15 mm o.d. cylindrical quartz furnace equipped with a 3 mm diameter chromel heating element regulated by a Bruker B−VT temperature controller. The radio frequency coil placed at the "magic angle" to the magnetic field was made from a copper capillary and cooled by a thermostated water flow.[12] An external jacket made of highly porous silica of low thermal conductivity was used to prevent heating of the magnet and also to minimize temperature gradients inside the heater. The use of a small volume of molten sample (approximately one-third of the volume of the sample tube) also diminished the temperature gradient over the sample, which did not exceed 5 K at 700 K.

The ^{133}Cs spectra were measured at a frequency of 52.5 MHz, a pulse width of 10 μs, and a delay between the pulses of 0.5 s. The ^{133}Cs chemical shifts were measured at room-temperature referenced to a 0.1 M aqueous solution of $CsNO_3$. The ^{17}O spectra were measured at a frequency of 54.2 MHz, a pulse width of 10 μs, and a delay between the pulses of 0.1 s. The ^{17}O chemical shifts measured at room temperature were referenced to H_2O.

Samples of around 3 g were contained in sealed quartz ampules. Before the measurements, all of the $Cs_2S_2O_7$−$CsHSO_4$ mixtures were kept molten at 500 °C for 3 h and quenched to room temperature to produce glasses.

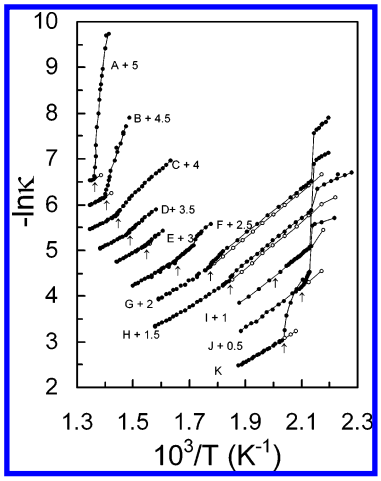

Figure 1. Electrical conductivity, κ, vs temperature for the $Cs_2S_2O_7$−$CsHSO_4$ system at various compositions $X(CsHSO_4)$: (A) 0.000, (B) 0.104, (C) 0.207, (D) 0.297, (E) 0.401, (F) 0.500, (G) 0.602, (H) 0.705, (I) 0.800, (J) 0.899, and (K) 1.000. The curves have been offset by the specified values. Open circles indicate subcooling, and arrows indicate liquidus temperatures.

Raman Spectroscopy. The cells used for Raman spectroscopy consisted of two concentric borosilicate test tubes (Ø = 4.0 and 6.0 mm).[13] The inner tube was inserted in the outer tube after filling the outer tube with chemicals. Both walls were sealed simultaneously. In this way the volume above the sample could be minimized, and thus, the absolute amount of H_2O escaping from the melt to the gas phase could be kept low. Because sealing of the tube had to be done before melting, an unavoidable dead space volume occurred, the size of which was a factor of 0.5−2 compared to the volume of the condensed phase, after melting. Raman spectra were measured with a DILOR XY spectrometer using the macro entrance. Spectra were excited with an Ar^+ ion laser of about 500 mW power at 514.5 nm wavelength. The exciting beam was vertically polarized, and the scattering plane was horizontal. The Rayleigh line was filtered off by using a Kaiser holographic SuperNotch-Plus filter (approximately 200 cm^{-1} cut-off). The Raman light was dispersed onto a liquid-nitrogen-cooled CCD detector by use of an 1800 lines/mm grating in an 800 mm focal length single spectrograph or in a second spectrograph with a much shorter focal length and a grating with 600 lines/mm. In both cases, the horizontal slits were set to 100 μm corresponding to a spectral resolution of 4−5 cm^{-1}. A sheet Polaroid analyzer, which permitted vertically or horizontally polarized light to pass, followed by a quarter wave depolarizer, was used to obtain polarization data. Calibration of the wavenumber scale was achieved with neon lines superimposed on the spectra, and wavenumbers reported are believed to be accurate within about 0.2 cm^{-1} for sharp bands. The accuracy of the temperature at the sample position was estimated to be ±5 K.

Results and Discussion

Conductivity Measurements. The specific conductivity, κ, of the $Cs_2S_2O_7$−$CsHSO_4$ system has been measured at 20 different compositions in the range 430−750 K. Results for selected compositions are plotted as $-\ln(\kappa)$ vs $1000/T$ in Figure 1. Conductivities in the liquid phase can be seen as slightly curved lines in the high temperature region. For each composition, a temperature range slightly above the liquidus temperature was chosen. The reason not to exceed far from this point was to avoid breaking the cell. This can happen either due to expansion of solidified matter when heating from too low a

TABLE 1: Coefficients for Empirical Equations[a] for the Specific Conductivities of Different Compositions, $X(CsHSO_4)$, of the $Cs_2S_2O_7-CsHSO_4$ System, Their Liquidus Temperatures, T_{liq}, and the Middle Temperature, T_m, of the Measured Temperature Range[b]

$X(CsHSO_4)$	T_{liq} (K)	T_m (K)	$A(X)$ (Ohm^{-1} cm^{-1})	$B(X)\cdot10^3$ (Ohm^{-1} cm^{-1})	$C(X)\cdot10^6$ (Ohm^{-1} cm^{-1})	ESD (Ohm^{-1} cm^{-1})
1.000	492	518	0.0691	0.9540	4.5317	0.000 18
0.899	476	506	0.0436	0.7322	3.4189	0.000 01
0.800	491	509	0.0395	0.7187	2.8226	0.000 08
0.705	544	608	0.1270	1.1966	1.0719	0.000 12
0.602	579	598	0.1074	1.1244	1.6746	0.000 25
0.500	617	621	0.1251	1.1896	2.4757	0.000 04
0.401	649	668	0.1428	1.0883	2.1263	0.000 13
0.297	675	701	0.1852	1.2246	0.6735	0.000 17
0.207	695	718	0.1993	1.2469	1.2791	0.000 33
0.104	716	723	0.1994	1.2510	−1.0150	0.000 66
0.000	735	738	0.2108	1.3352	3.9871	0.000 39

[a] $\kappa = A(X) + B(X)(T - T_m) + C(X)(T - T_m)^2$, $T \geq T_{liq}$. [b] Consult Figure 1 for the highest measuring temperature.

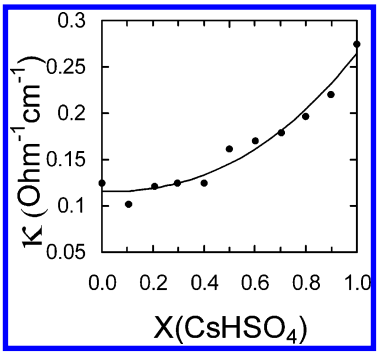

Figure 2. Conductivity isotherm for the $Cs_2S_2O_7-CsHSO_4$ system at 650 K. The curve corresponds to the fitted expression $\kappa = 0.1136 - 0.0070X + 0.1114X^2 + 0.0450X^3$ (Ohm^{-1} cm^{-1}) with a regression coefficient of $R^2 = 0.965$.

temperature (for the $Cs_2S_2O_7$ side of phase diagram) or to avoid explosion due to evolved water vapor pressure at high temperatures ($CsHSO_4$ side of phase diagram). As previously,[2] we have fitted polynomials of the form $\kappa(X) = A(X) + B(X)(T - T_m) + C(X)(T - T_m)^2$ to the conductivities of the liquid regions measured for the selected compositions of Figure 1. The results are given in Table 1. T_m is an arbitrarily selected temperature in the middle of the measured range as indicated in Table 1. Inter- or extrapolated values corresponding to $T = 650$ K have been plotted vs mol fraction of $CsHSO_4$ along with a polynomial fit in Figure 2. It seems evident that the conductivity increases with the molar fraction of $CsHSO_4$ as expected mainly because of the high mobility of H^+ ions. A similar tendency was earlier observed for the analogous Na and K based systems.[1,2]

Thermal Measurements. Because of the large difference between the melting point of the pure salts (492 and 735 K respectively for $CsHSO_4$ and $Cs_2S_2O_7$) and the thermal decomposition of $CsHSO_4$ above the melting point, it was impossible to determine the enthalpy of mixing over the full composition range. However, in the assessment of the calculations of the thermodynamic data obtained for this system, the partial excess thermodynamic functions are taken into account, and it seemed more reasonable to measure directly the partial enthalpies of mixing of $Cs_2S_2O_7$ in the melts. The partial excess enthalpy ΔH^E has been measured at

$$X(Cs_2S_2O_7) = 0.03,\ T = 517\ K;$$
$$X(Cs_2S_2O_7) = 0.51,\ T = 670\ K;$$
$$X(Cs_2S_2O_7) = 0.53,\ T = 670\ K$$

For each composition, the partial excess enthalpy has been measured three times. The scattering was found to be less than ±1.5%. We obtained $\Delta H^E(Cs_2S_2O_7) = -12279$, -5635, and -6985 J mol^{-1} for $X(Cs_2S_2O_7) = 0.03$, 0.51, and 0.53, respectively.

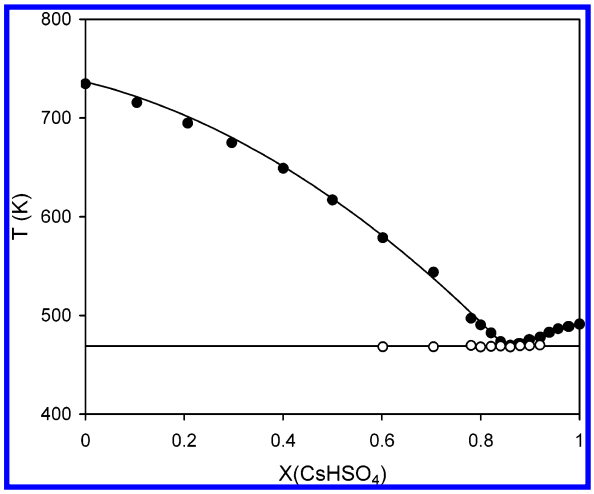

Figure 3. Phase diagram of the $Cs_2S_2O_7-CsHSO_4$ system based on data from conductivity measurements. Open symbols indicate the solidus line (temperature of fusion of the eutectic).

The composition of the eutectic melt obtained by DSC was $X(CsHSO_4) = 0.87$ with a melting point of 468 K, and the heat of fusion was equal to 10 740 J mol^{-1}. From the experiments, we obtained also the solid−solid transition of pure $CsHSO_4$ to take place at 415 K, in good agreement with the value (414 K) obtained in this work by NMR. The associated heat of transition was found to be equal to $\Delta_{trans}H$ ($CsHSO_4$) = 6000 J mol^{-1}.

Phase Diagram. The phase diagram of the binary system $CsHSO_4-Cs_2S_2O_7$ is displayed in Figure 3. The points on the liquidus curve in the phase diagram have been determined by obtaining the temperatures of complete melting for all of the 20 different compositions measured by electrical conductivity measurements. The solidus and liquidus temperatures obtained for all measurements are given in Table 2. The melting point of pure $Cs_2S_2O_7$ was found to be 735 K which is in good agreement with our previous investigation.[4] As for pure $CsHSO_4$, the melting point was measured to be 492 K, a value that to our knowledge has not been reported before. Twelve of the compositions were chosen to be within the range $X(CsHSO_4) = 0.78-1.00$ in order to achieve an accurate determination of the eutectic composition. At compositions in the vicinity of the eutectic, the solidus temperature could still be observed. Because no peritectic compounds are formed, the solidus line is probably representative for the whole composition range as also was the case for the Na and K equivalents of the present binary Cs system but were not investigated here due to the above-mentioned risk of breaking the cell by cooling too far below

TABLE 2: Liquidus, T_{liq}, and Solidus, T_{sol}, Temperatures Found from Conductivity Measurements at the Indicated Compositions, $X(CsHSO_4)$, of the $Cs_2S_2O_7-CsHSO_4$ System

$X(CsHSO_4)$	T(solidus) [K]	T(liquidus) [K]
1.000		492
0.977		489
0.957		487
0.938		483
0.920	470	478
0.899	470	476
0.880	469	472
0.860	468	470
0.840	469	474
0.821	469	482
0.800	468	491
0.780	470	497
0.705	468	544
0.602	468	579
0.500		617
0.401		649
0.297		675
0.207		695
0.104		716
0.000		735

the liquidus temperature. The eutectic composition was found to be $X(CsHSO_4) = 0.86$ with a melting point of 470 K. For the analogous Na and K systems, the eutectics were found at $X(NaHSO_4) = 0.97$ and $X(KHSO_4) = 0.94$. Preliminary[3] results for the Rb system seem to point to an eutectic at $X(RbHSO_4) = 0.87$. Thus, increasing the size of the alkali cation apparently decreases the mol fraction $X(MHSO_4)$ for the eutectic compositions.

For the liquidus curve, we have used the classical equation deduced from the equality of the chemical potential of the component, A, in the pure solid phase and in the liquid phase

$$-\Delta\bar{G}_{fus}(A,T) = RT \ln X(A) + \Delta\bar{G}^{E}_{T}(A,l)$$

where $X(A)$ is the composition of A in the liquid phase. The Gibbs free energies of fusion of $Cs_2S_2O_7$ and $CsHSO_4$ are calculated from our measured values[3] of $C_p(s)$, $C_p(l)$, ΔH_{fus}, and T_{fus}. For $CsHSO_4$, the temperature range is very short, and we have considered the term $\Delta C_p = C_p(l) - C_p(s)$ equal to zero.

The excess Gibbs energy is obtained from the empirical expression[2]

$$\Delta G^{E}(T) = X(1-X)(A_0 + A_1T + A_2T(1 - \ln T)) + X(B_0 + B_1T + B_2T(1 - \ln T))$$

where

$$X = X(CsHSO_4)$$

From this expression by using the Helmholtz relation, we can deduce the excess enthalpy

$$\Delta H^{E}(X) = X(1-X)(A_0 + A_1T + X(B_0 + B_1T))$$

From these relations, all six coefficients are calculated by a multilinear regression method using the 20 experimental liquidus points and the three experimental values of the partial excess enthalpy of $Cs_2S_2O_7$. We obtain the values

$$A_0 = -96.89 \text{ kJ}; \quad A_1 = 11.71 \text{ kJ T}^{-1}; \quad A_2 = 1.86 \text{ kJ T}^{-2}$$

$$B_0 = 60.36 \text{ kJ}; \quad B_1 = -8.25 \text{ kJ T}^{-1}; \quad B_2 = -1.34 \text{ kJ T}^{-2}$$

The regression coefficient is equal to 0.998.

From these coefficients, we can calculate the excess enthalpy and the phase diagram

$$\Delta H^{E}(Cs_2S_2O_7 \text{ at } X(Cs_2S_2O_7) = 0.03) = -12225 \text{ J mol}^{-1}$$
(experimental: -12279 J mol^{-1})

$$\Delta H^{E}(Cs_2S_2O_7 \text{ at } X(Cs_2S_2O_7) = 0.51) = -5706 \text{ J mol}^{-1}$$
(experimental: -5635 J mol^{-1})

$$\Delta H^{E}(Cs_2S_2O_7 \text{ at } X(Cs_2S_2O_7) = 0.53) = -6985 \text{ J mol}^{-1}$$
(experimental: -6985 J mol^{-1})

Thus, a very good agreement is found between the calculated and measured value of $\Delta H^{E}(Cs_2S_2O_7)$. The calculated liquidus curve is shown on the phase diagram in Figure 3. A good fit to the experimental data points is observed. The calculated position of the eutectic $X(CsHSO_4) = 0.865$, $T = 469$ K agrees well with our experimental values of $X(CsHSO_4) = 0.86$ and its temperature of fusion of 470 K.

NMR Spectroscopic Observations. A single resonance line with a line width of about 300 and 150 Hz is respectively observed in the ^{17}O and ^{133}Cs NMR spectra at 735 K for all of the $Cs_2S_2O_7-CsHSO_4$ samples, i.e., in the range $X(CsHSO_4) = 0-1$. The chemical shifts vary from 206 to 193 ppm and from -5.5 to -10 ppm for the ^{17}O and ^{133}Cs NMR spectra, respectively. The observation of a single line in the ^{17}O NMR spectra indicates a rapid exchange of oxygen atoms between the different species in the melt. In agreement with previous results,[14] no separate lines from bridging and terminal oxygens in the pyrosulfate anions have been detected, most probably due to equilibria that include a fast dissociation and recombination of the pyrosulfate anions, e.g., $S_2O_7^{2-} \leftrightarrows SO_4^{2-} + SO_3$. The rate of this process is probably more than 10^3 Hz as estimated from the expected difference in chemical shifts of bridging and terminal oxygens. Similar considerations can be put forward for the hydrogen sulfate anion, where the fast proton exchange reaction $HSO_4^- \leftrightarrows SO_4^{2-} + H^+$ can account for the observation of only one ^{17}O NMR in molten $CsHSO_4$.[2] No other signals, e.g., from H_2O, have been detected in the ^{17}O NMR spectra. This can be due either to a small concentration of H_2O or a rapid equilibrium process (e.g., $2HSO_4^- \leftrightarrows S_2O_7^{2-} + H_2O$), which averages the signals from water oxygen with those from the hydrogen sulfate and pyrosulfate oxygens. A narrow single line in the ^{133}Cs NMR spectra, with the same chemical shift in the melts of different compositions, indictaes an identical chemical state of Cs. Thus, dissociation of both $CsHSO_4$ and $Cs_2S_2O_7$ seems to take place with the formation of Cs^+ cations with very weak ion association and high mobility in both types of melts.

Previously, we have demonstrated that ^{133}Cs NMR spectra are very informative regarding the phase transitions in $Cs_2S_2O_7$ and in $CsHSO_4$.[8,12] Measurements of spectra during sample heating or cooling lead to detailed schemes on the phase transitions in all of the samples as well as to ascribe the observed phases to these already known. The schemes of the phase transitions of $Cs_2S_2O_7$ and $CsHSO_4$ found during sample heating and cooling are shown in Figure 4.

Heating of Solid $Cs_2S_2O_7$. As the starting point at room-temperature, we have a polycrystalline phase ($Cs_2S_2O_7$—II, obtained by thermal decomposition of $Cs_2S_2O_8$). In accordance with previous data,[12] the static spectrum of $Cs_2S_2O_7$ consists of a broadened line (about 5 kHz) which is a superposition of 10 lines from unequivalent Cs atoms in the structure of this

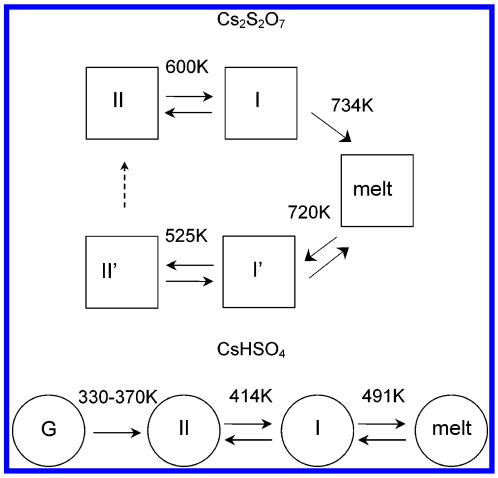

Figure 4. Schemes showing phase transitions in $Cs_2S_2O_7$ and $CsHSO_4$. $Cs_2S_2O_7$ is indicated as rectangles, and $CsHSO_4$ is indicated as circles. Both I and I′ indicate the superionic phases found in $Cs_2S_2O_7$ and $CsHSO_4$. II indicates thermodynamically stable phases. Dotted arrows correspond to the transition taking place during $Cs_2S_2O_7$ milling.

TABLE 3: ^{133}Cs NMR Parameters of Different Phases of $Cs_2S_2O_7$ and $CsHSO_4$ in Pure Compounds and in $Cs_2S_2O_7-CsHSO_4$ Mixed Samples

phase	nucleus	σ_{iso}, ppm	C_Q, kHz	η_Q	η_s	$\Delta\sigma$, ppm	ΔC_Q, kHz
$Cs_2S_2O_7-II$	Cs_1	−57.7	310	0.67			
	Cs_2	−47.2	310	0.67			
	Cs_3	−40.3	310	0.67			
	Cs_4	−38.3	310	0.67			
	Cs_5	−32.8	310	0.67			
	Cs_6	−15.5	310	0.67			
	Cs_7	−11.3	310	0.67			
	Cs_8	−11.3	310	0.67			
	Cs_9	5.1	310	0.67			
	Cs_{10}	14.5	310	0.67			
$Cs_2S_2O_7-I$		2.3	220	0.19	0.35	−15	
$Cs_2S_2O_7-I$ in $Cs_2S_2O_7-CsHSO_4$		12	245	0.09	*a*	*a*	
$Cs_2S_2O_7-I'$		−11.3	425	0.05	*a*	3	30
$Cs_2S_2O_7-I'$ in $Cs_2S_2O_7-CsHSO_4$		−20	466	0	*a*	3	1
		$\Delta\sigma_{iso} = 1$					
$CsHSO_4-I$		−14.0	253	0	0.15	−19	
$CsHSO_4-I$ in $Cs_2S_2O_7-CsHSO_4$		−10	245	0	*a*	*a*	
		$\Delta\sigma_{iso} = 1$					
$CsHSO_4-II$		−19.5	185	1.0	0.5	15	

[a] Value uncertain due to superposition of the melt spectrum.

compound (see Table 3). The progressive increase of the temperature results in a narrowing of the line due to the increase of the mobility of the Cs cations in the crystal lattice. In the temperature range from 500 to 600 K, a symmetric line, with a position that is close to the average position of lines from the most populated Cs sites, is observed. This indicates that the cation mobility occurs as jumps between Cs sites and begins at these temperatures. Further increase of the temperature transformed this spectrum to one typical for axial anisotropy of the chemical shielding tensor,[8] and at the same time, the first-order quadrupole transitions appeared in the spectra (superionic conducting phase $Cs_2S_2O_7-I$, see Table 3). Above the melting point of $Cs_2S_2O_7$, a single narrow line typical for a liquid appeared in the spectra ($Cs_2S_2O_7$ −melt). The chemical shift slightly decreased by increasing of temperature.

Cooling of Molten $Cs_2S_2O_7$. In general, the behavior of the ^{133}Cs NMR spectra were very similar to those obtained by heating of the powdered $Cs_2S_2O_7$ sample; nevertheless, some features should be mentioned. In the temperature range from 700 to 600 K, the axial anisotropy of the observed line differed from that in $Cs_2S_2O_7-I$ by the sign of anisotropy of the magnetic shielding tensor and the position of the quadrupole satellite transitions (superionic conducting phase $Cs_2S_2O_7$ −I′, see Table 3). At room-temperature the ^{133}Cs NMR spectrum of the crystalline $Cs_2S_2O_7$ sample obtained from the melt differs from that of the powdered $Cs_2S_2O_7-II$ prepared by thermal decomposition of $Cs_2S_2O_8$. It is remarkable that milling of the crystalline sample restored the phase $Cs_2S_2O_7-II$. Therefore, we conclude that the room-temperature phase, obtained after slow cooling of the melt, is a different phase ($Cs_2S_2O_7-II'$).

Heating of Solid $CsHSO_4$. To start with in this case, we had an amorphous phase $CsHSO_4-G$, obtained by adding carefully weighed amounts of water to $Cs_2S_2O_7-II$. Slow heating of the sample up to 330−370 K lead to the thermodynamically stable phase II ($CsHSO_4-II$, see Table 3), that at 414 K transformed to the superionic conducting phase ($CsHSO_4-I$, see Table 3) which melted at 491 K ($CsHSO_4$-melt).

Cooling of Molten $CsHSO_4$. The behavior by cooling was the same as observed for the powdered sample during heating, the only difference was that the thermodynamically stable phase II was the last in this chain. This scheme is in good agreement with literature data.[15−18]

Similarly, the behavior of the mixed samples were investigated. As an example the ^{133}Cs NMR spectra of a sample of composition $X(CsHSO_4) = 0.2$ measured by progressive increase of the temperature from 300 to 700 K and subsequent decrease from 700 to 300 K are shown in Figure 5 and in the scheme presented in Figure 7. The spectrum of the melt-quenched glassy sample at ambient temperature showed a broad line (Figure 5, 300 K), that did not narrow under MAS conditions. The latter is caused by a random distribution of different Cs sites, and the ^{133}Cs NMR central line was composed of a large number of individual transition frequencies overlapping in a broad unresolved line. The progressive increasing of the temperature was accompanied by a glass-to-crystal transition at 410 K and a spectrum typical for a super-ionic conducting phase of $CsHSO_4-I$ (Figures 5 and 6, Table 3) appeared. The latter phase was observed in the range 410−470 K (Figure 5).

Above 470 K, a narrow line of liquid ($CsHSO_4$-melt) appeared, at 10 ppm, with a gradually increasing intensity up to 665 K (Figure 5). It is remarkable that the increase of the temperature leads to the appearance at 665 K of the super-ionic conducting phase of ($Cs_2S_2O_7-I'$) exhibiting a NMR line with clear quadrupolar transitions of the first order (Table 3, Figures 5 and 6). At 700 K, a narrow line of liquid $Cs_2S_2O_7$ appeared. Above 700 K, the intensity of the spectrum remained almost constant (slowly decreasing according to the Curie law), indicating that the sample ($Cs_2S_2O_7-CsHSO_4$) was completely molten (Figure 5), in accordance with the phase diagram (Figure 3).

The features of the spectra by decreasing the temperature in the range 710−300 K were very similar to what has been described regarding heating. The differences that were revealed in the behavior of, e.g., the sample $X(CsHSO_4) = 0.2$ during cooling and heating were the following: The NMR parameters of the super-ionic conducting phase during sample cooling were close to those of $Cs_2S_2O_7-I$ (see Table 3), whereas under heating, they were close to $Cs_2S_2O_7-I'$. By slow cooling below T_g (the glass-to-crystal transition temperature), a polycrystalline phase was formed.

These differences can be understood from the dependence of the chemical shift on the temperature. Below T_g, a different

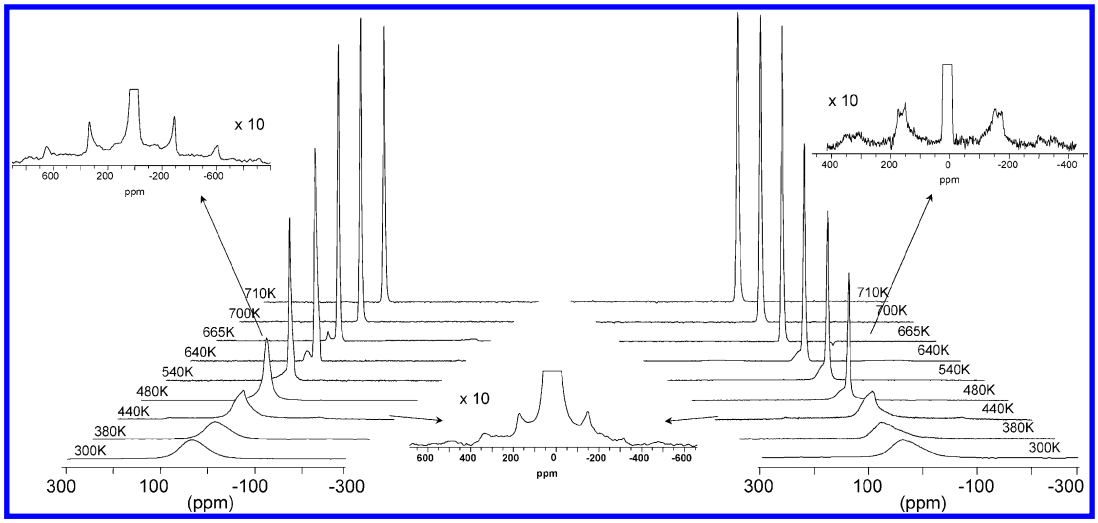

Figure 5. ^{133}Cs NMR spectra of the $Cs_2S_2O_7-CsHSO_4$ system for $X(CsHSO_4) = 0.2$ obtained by increase (left) and decrease (right) of the temperature of the glassy sample in the range 300−700 K. The inserted spectra of superionic phases of $Cs_2S_2O_7$ and $CsHSO_4$ are shown to the left ($Cs_2S_2O_7-I'$), to the right ($Cs_2S_2O_7-I$), and in the middle ($CsHSO_4-I$).

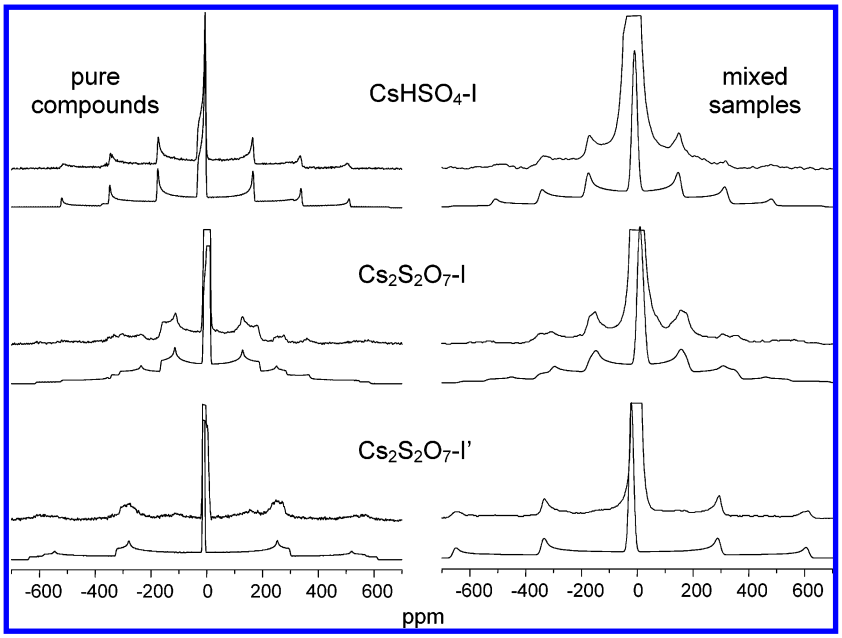

Figure 6. Experimental and simulated ^{133}Cs NMR spectra of the superionic conducting phases, $CsHSO_4-I$, $Cs_2S_2O_7-I$, and $Cs_2S_2O_7-I'$, in pure compounds (left) and in mixed $Cs_2S_2O_7-CsHSO_4$ samples (right). NMR parameters are given in Table 3.

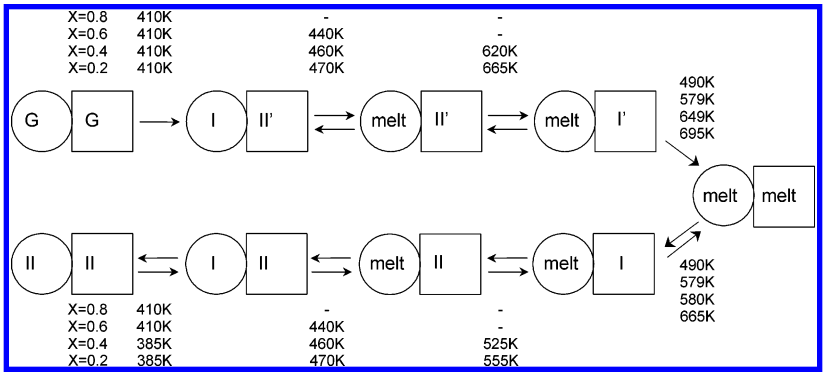

Figure 7. Scheme showing the phase transitions in $Cs_2S_2O_7-CsHSO_4$ samples at different compositions $X(CsHSO_4)$. $Cs_2S_2O_7$ phases are shown as rectangles, and $CsHSO_4$ is shown as circles. I and I′ indicate the superionic phases found in $Cs_2S_2O_7$ and $CsHSO_4$, and II indicates thermodynamically stable phases.

state of the sample existed: Initially (by increase in temperature), the melt-quenched sample was in a glassy state, whereas after cooling, a polycrystalline sample was formed. The difference observed above T_g must be due to the different super-ionic phases: $Cs_2S_2O_7-I'$ (heating) and $Cs_2S_2O_7-I$ (cooling) (Figures 5 and 6).

If we compare the schemes of mixed and pure samples (Figures 4 and 7), the following difference in behavior can be noted:

Slow cooling of $Cs_2S_2O_7$ leads to the formation of a superionic conducting phase $Cs_2S_2O_7-I'$, whereas for all mixed samples, slow cooling leads to the superionic conducting phase $Cs_2S_2O_7-I$. The latter phase ($Cs_2S_2O_7-I$) for pure $Cs_2S_2O_7$ is formed only from the polycrystalline sample and never from molten $Cs_2S_2O_7$. These results clearly indicate a fast amorphization of pure $Cs_2S_2O_7$ by cooling of the melt, whereas heating of the melt-quenched glassy mixtures leads to formation of the superionic conducting phase ($Cs_2S_2O_7-I'$). The other superionic conducting phase $Cs_2S_2O_7-I$ appears in all mixed samples during slow cooling of the melts, thus demonstrating that there is no amorphization of the sample. Thus, it appears that polycrystalline samples are formed after cooling of mixed samples. All of these transformations are summarized in the schemes, in Figures 4 and 7.

Comparison of NMR parameters of the pure super-ionic conducting phases, $CsHSO_4-I$, $Cs_2S_2O_7-I$, and $Cs_2S_2O_7-I'$, with those observed in mixed samples (see Table 3 and Figure 6) indicates that they are quite similar, regarding structures and mobility. The values of the NMR parameters obtained for all of the phases make it possible to estimate the rate of Cs^+ exchange in the different phases. For glassy samples as well as for polycrystalline samples, this exchange is very slow, whereas for the temperature ranges where the superionic conducting phases exist simultaneously with the liquid phase, the rate of the exchange process between these phases is determined by the mobility of Cs^+ cations in the superionic phase. The dependency of the chemical shift upon temperature for all heated samples shows characteristic changes corresponding to the glass crystal transitions (T_g) of $CsHSO_4$ and $Cs_2S_2O_7$, the phase transition II → I of $CsHSO_4$, and the solid-to-liquid transitions of $CsHSO_4$ and $Cs_2S_2O_7$ in the pure compounds.

The changes in the intensity upon temperature for the ^{133}Cs NMR central line in the samples with $X(CsHSO_4) = 0$, 0.2, 0.4, 0.6, 0.8, and 1.0 are shown in Figure 8. The quadrupolar nuclei resonance line for solids consists of 2I superimposed components and the intensity of each component is proportional to $I(I + 1) - m(m - 1)$. Because Cs has a nuclear spin of 7/2, seven transitions with the relative intensities of 7:12:15:16:15:12:7 should be observed in the spectra of solid samples. In the present case, only the central transition (+1/2 to −1/2) is observed due to point defects; therefore, its intensity is equal to 4/21 of the total intensity arising from all possible transitions. In the liquid state, however, only a single line with the intensity equal to 1 is observed.

The signal intensity should be proportional to the fraction of liquid and solid phases. For the pure compounds, $Cs_2S_2O_7$ ($X(CsHSO_4) = 0$) and $CsHSO_4$ ($X(CsHSO_4) = 1.0$) a sharp increase of the intensity was observed at 734 and 491 K, respectively, in good agreement with the temperatures of fusion found in this work. Similar dependencies were observed for the mixed samples with $X(CsHSO_4) = 0.2-0.8$, where the maximum intensities of the NMR signal were obtained at temperatures in good agreement with the liquidus temperatures of the phase diagram. Furthermore, for the compositions $X(CsHSO_4) = 0.4$, 0.6, and 0.8, an onset of the increase of the signal intensity was found just below 470 K, i.e., at the temperature of fusion of the eutectic mixture, whereas for $X(CsHSO_4) = 0.2$ a too small amount of eutectic melt was formed to be observed by NMR.

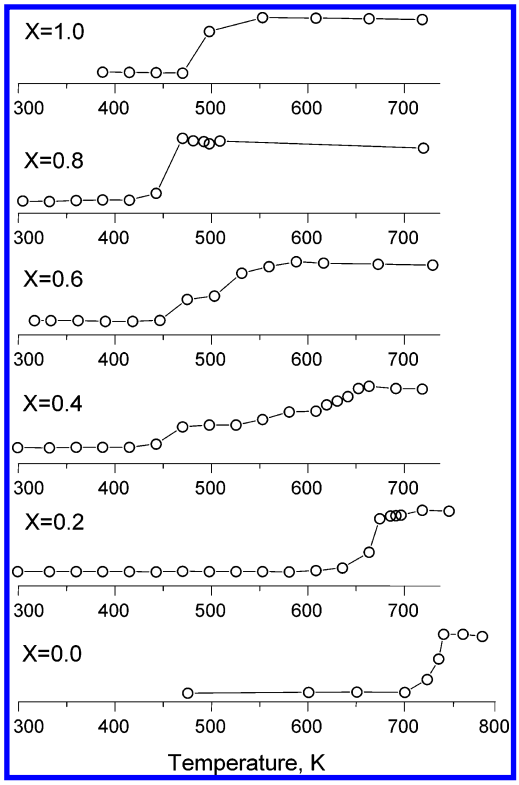

Figure 8. Integrated intensity of the central transition of the ^{133}Cs NMR spectra of the $Cs_2S_2O_7-CsHSO_4$ system at different temperatures for the composition range $X(CsHSO_4) = 0.0-1.0$.

Raman Spectra of the $Cs_2S_2O_7-CsHSO_4$ System. Mixtures of the two components with initial compositions $X(CsHSO_4) = 0$, 0.2, 0.4, 0.6, 0.8, and 1.0 were prepared and heated, until thermal equilibrium was reached. To avoid explosion of the glass cells due to high water vapor pressures, the samples with compositions $X(CsHSO_4) = 1.0$ and 0.8 were equilibrated and measured at 623 K, whereas for $X(CsHSO_4) = 0.6$ and 0.4, the measuring temperature was 673 K. The samples with $X(CsHSO_4) = 0.0$ and 0.2 were recorded at 736 K just above the melting point of $Cs_2S_2O_7$. Raman spectra are shown in Figure 9. The strongest bands of $Cs_2S_2O_7$ occur at approximately 1080, 725, and 315 cm^{-1}. For $CsHSO_4$ the most characteristic bands are seen at approximately 1050 cm^{-1} (ν S−O) and in the range 820−860 cm^{-1} (ν S−OH) where the latter band was temperature dependent. At room temperature, it was observed at 858 cm^{-1}, at 523 K (32 K above the melting point) it was observed at 850 cm^{-1}, and at 673 K, it occurred at 823 cm^{-1}. The band at around 840 cm^{-1} is also seen in $KHSO_4$ melts, and has been assigned[2,3] to the symmetric stretching involving the S−OH group. The temperature dependence can then be explained by a weakening of the hydrogen bonds with increasing temperature. Other bands from HSO_4^- are seen at 570 cm^{-1} ν_4 (S−O) and 410 cm^{-1} ν_2 (S−O), where ν_2 and ν_4 refer to modes in tetrahedral SO_4^{2-}.

As seen from the gradual change from one to the other component in Figure 9, no new intermediate compound is formed in the liquid phase. The Raman spectra in the region above 3000 cm^{-1} region (not shown in the figure) indicated that solvated H_2O was present, which formed according to the reaction $2HSO_4^- \leftrightarrows S_2O_7^{2-} + H_2O$. This equilibrium also accounts for the presence of bands due to $S_2O_7^{2-}$ in the spectrum of pure molten $CsHSO_4$ at 623 K (Figure 9) well above the melting point of the salt. In the spectral region 0−1500 cm^{-1}, all observed bands could be attributed to either $S_2O_7^{2-}$ or HSO_4^- in the entire composition range.

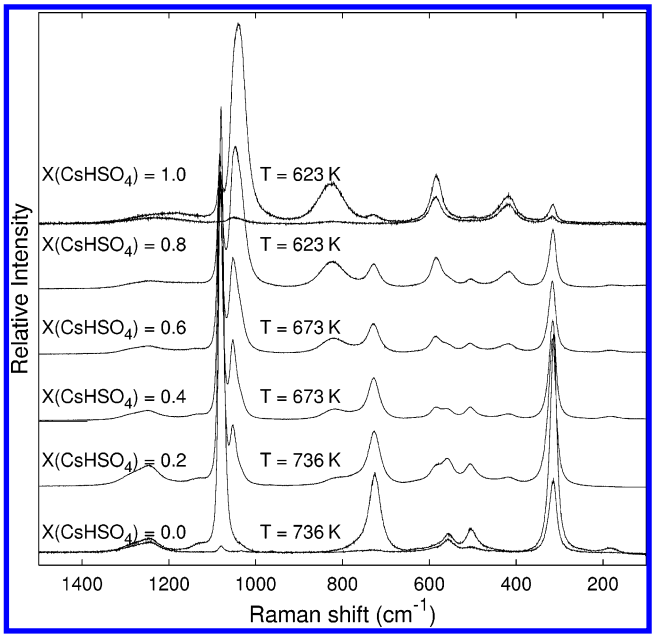

Figure 9. Raman spectra of molten $Cs_2S_2O_7-CsHSO_4$ samples in the temperature range 623−736 K. For the spectra of pure components, both vertical−vertical and vertical−horizontal polarizations are shown. For all others, only spectra with vertical−vertical polarization recordings are plotted.

Acknowledgment. The Danish Technical Science Research Foundation, Corrit Foundation, Tuborg Foundation, Danfoss A/S, Thomas B. Thrige Foundation, P. A. Fiskers Foundation, NATO (Science for Peace Project SFP 971984), Energi E2 A/S and Director Henriksen's Foundation are acknowledged for financial support and for grants which made this research possible.

References and Notes

(1) Hatem, G.; Gaune-Escard, M.; Rasmussen, S. B.; Fehrmann, R. *J. Phys. Chem. B* **1999**, *103* 1027.
(2) Eriksen, K. M.; Fehrmann, R.; Hatem, G.; Gaune-Escard, M.; Lapina, O. B.; Mastikhin, V. M. *J. Phys. Chem.* **1996**, *100*, 10771.
(3) Hatem, G.; Eriksen, K. M.; Gaune-Escard, M.; Fehrmann, R. *Top. Catal.* **2002**, *19*, 323.
(4) Folkmann, G. E.; Hatem, G.; Fehrmann, R.; Gaune-Escard, M.; Bjerrum, N. J. *Inorg. Chem.* **1991**, *30*, 4057.
(5) Folkmann, G. E.; Hatem, G.; Fehrmann, R.; Gaune-Escard, M.; Bjerrum, N. J. *Inorg. Chem.* **1993**, *32*, 1559.
(6) Nielsen, K.; Fehrmann, R.; Eriksen, K. M. *Inorg. Chem.* **1993**, *32*, 4825.
(7) Lapina, O. B.; Mastikhin, V. M.; Shubin, A. A.; Eriksen, K. M.; Fehrmann, R. *J. Mol. Catal. A* **1995**, *99*, 123.
(8) Lapina, O. B.; Terskikh, V. V.; Shubin, A. A.; Mastikhin, V. M.; Eriksen, K. M.; Fehrmann, R. *J. Phys. Chem. B* **1997**, *101*, 9188.
(9) Rasmussen, S. B.; Eriksen, K. M.; Fehrmann, R. *J. Phys. Chem. B* **1999**, *103*, 11282.
(10) Hatem, G.; Eriksen, K. M.; Fehrmann, R. *Thermochim. Acta* **2001**, *379*, 187.
(11) Boghosian, S.; Chrissanthopoulos, A.; Fehrmann, R. *J. Phys. Chem. B* **2002**, *106*, 49.
(12) Lapina, O. B.; Terskikh, V. V.; Shubin, A. A.; Eriksen, K. M.; Fehrmann, R. *Colloids Surf. A* **1999**, *158*, N 1−2 255.
(13) Rasmussen, S. B.; Berg, R. W.; Fehrmann, R. *Prog. Molten Salt Chem.*, **2000**, *1*, 449.
(14) Lapina O. B.; Mastikhin V. M.; Shubin A. A.; Krasilnikov V. N.; Zamaraev K. I. *Prog. NMR Spectrosc.* **1992**, *24*, 457.
(15) Chisholm, C. R. I.; Haile, S. M. *Mater. Res. Bull.* **2000**, *35*, 999.
(16) Iton, K.; Ozaki, T.; Nakamura, E. *Acta Crystallogr.* **1981**, *B37*, 1908.
(17) Damyanovich, A.; Pintar, M. M. *Phys. Rev. B* **1997-I**, *56*, 7942.
(18) Arcon, A.; Blinc, R.; Dolinsek, J. *Phys. Rev. B* **1997-II**, *55*, 8961.